Atmospheric Environment 173 (2018) 6–15

Contents lists available at ScienceDirect

Atmospheric Environment

journal homepage: www.elsevier.com/locate/atmosenv

Mercury from wildfires: Global emission inventories and sensitivity to 2000–2050 global change

Aditya Kumar[a,b], Shiliang Wu[a,b,c,*], Yaoxian Huang[a,d], Hong Liao[e], Jed O. Kaplan[f]

[a] Department of Geological and Mining Engineering and Sciences, Michigan Technological University, Houghton, MI, USA
[b] Department of Civil and Environmental Engineering, Michigan Technological University, Houghton, MI, USA
[c] School of Environment and Energy, Peking University Shenzhen Graduate School, Shenzhen, China
[d] Now at Department of Climate and Space Sciences and Engineering, University of Michigan, Ann Arbor, MI 48109, USA
[e] School of Environmental Science and Engineering, Nanjing University of Information Science & Technology, Nanjing, China
[f] ARVE Research SARL, Pully, Switzerland

GRAPHICAL ABSTRACT

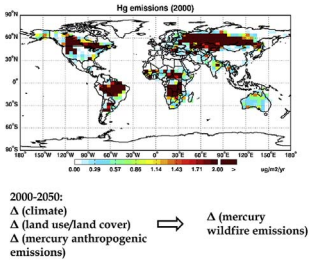

ARTICLE INFO

Keywords:
Biomass burning
Modeling
Climate change
Land use
Land cover

ABSTRACT

We estimate the global Hg wildfire emissions for the 2000s and the potential impacts from the 2000–2050 changes in climate, land use and land cover and Hg anthropogenic emissions by combining statistical analysis with global data on vegetation type and coverage as well as fire activities. Global Hg wildfire emissions are estimated to be 612 Mg year^{-1}. Africa is the dominant source region (43.8% of global emissions), followed by Eurasia (31%) and South America (16.6%). We find significant perturbations to wildfire emissions of Hg in the context of global change, driven by the projected changes in climate, land use and land cover and Hg anthropogenic emissions. 2000–2050 climate change could increase Hg emissions by 14% globally and regionally by 18% for South America, 14% for Africa and 13% for Eurasia. Projected changes in land use by 2050 could decrease the global Hg emissions from wildfires by 13% mainly driven by a decline in African emissions due to significant agricultural land expansion. Future land cover changes could lead to significant increases in Hg emissions over some regions (+32% North America, +14% Africa, +13% Eurasia). Potential enrichment of terrestrial ecosystems in 2050 in response to changes in Hg anthropogenic emissions could increase Hg wildfire emissions globally (+28%) and regionally (+19% North America, +20% South America, +24% Africa, +41% Eurasia). Our results indicate that the future evolution of climate, land use and land cover and Hg anthropogenic emissions are all important factors affecting Hg wildfire emissions in the coming decades.

* Corresponding author. Department of Geological and Mining Engineering and Sciences, Michigan Technological University, Houghton, MI, USA.
E-mail address: slwu@mtu.edu (S. Wu).

http://dx.doi.org/10.1016/j.atmosenv.2017.10.061
Received 29 June 2017; Received in revised form 11 October 2017; Accepted 28 October 2017
Available online 31 October 2017

1. Introduction

Mercury (Hg) is a toxic and persistent pollutant in the global environment. Hg emitted to the atmosphere can be transported long distances before depositing to terrestrial and aquatic systems. The atmospheric emissions of Hg include both anthropogenic sources such as fossil fuel combustion, smelting of ores, cement production, waste incineration, and artisanal gold mining (Chen et al., 2014; Pacyna et al., 2010; Pirrone et al., 2010; Streets et al., 2011; Veiga et al., 2006), natural emissions from erupting and passively degassing volcanoes, geothermal hot springs, topsoil enriched in Hg (Ferrara et al., 2000; Nimick et al., 2013; Nriagu and Becker, 2003; Pyle and Mather, 2003; Varekamp and Buseck, 1986), and biomass burning/wildfires (Friedli et al., 2003, 2009; Sigler et al., 2003; Turetsky et al., 2006; Veiga et al., 1994; Weiss-Penzias et al., 2007; Wiedinmyer and Friedli, 2007).

Terrestrial vegetation plays an important role in the biogeochemical cycling of Hg, and is considered a significant reservoir for atmospheric Hg. Obrist (2007) estimated the global uptake of atmospheric Hg by vegetation could be more than 1 000 Mg per year. Retention of atmospheric Hg by vegetation delays its transport to soils and aquatic systems (Graydon et al., 2012). Hence, vegetation plays an important role in Hg sequestration by terrestrial ecosystems. Wildfires, through the burning of biomass, can effectively mobilize the Hg stored in terrestrial ecosystems and lead to massive emissions of Hg and other pollutants into the atmosphere (Andreae and Merlet, 2001; Biswas et al., 2007; Ito and Penner, 2004; Turetsky et al., 2006; van der Werf et al., 2006; Veiga et al., 1994). Multiple studies have estimated Hg wildfire emissions at the global and regional scales (Table 2) with global total emissions in the range of 104–1 330 Mg Hg $year^{-1}$ indicating large uncertainty in the estimated Hg emissions from wildfires. A number of studies have developed wildfire emission inventories for Hg based on CO or CO_2 emission inventories by applying fixed emission ratios between Hg and CO/CO_2 [e.g (Brunke et al., 2001; Ebinghaus et al., 2007; Sigler et al., 2003).]. To our knowledge, Friedli et al. (2009) is the only study so far that have compiled a multi-year (1997–2006) emission inventory for Hg from wildfires at the global scale by accounting for the variations in Hg emission factors across geographical regions and ecosystems. The emission factor (EF) for a given species (Hg in this case) can be expressed as the mass of that species emitted per unit dry biomass burned (Andreae and Merlet, 2001). It is affected by both the vegetation type and geographical region.

Significant changes in global vegetation coverage are expected in the coming decades driven by either climate change (referred to as land cover change hereon) or anthropogenic land use change (referred to as land use change hereon) (Bachelet et al., 2001, 2003; Cox et al., 2000; Falloon et al., 2012; Notaro et al., 2007; O'ishi and Abe-Ouchi, 2009; Tilman et al., 2001; Wu et al., 2012). Wu et al. (2012) predicted significant changes in forests and grassland coverage by 2050 with the northern mid-latitudes being affected the most. Notaro et al. (2007) predicted reduced forest cover over the Amazon, South Africa and Australia due to the radiative effect of rising CO_2 and poleward shift of the boreal forest due to both radiative and physiological effects. In addition, continued anthropogenic conversion of forested land for agriculture in the future to support a growing global human population and the resulting food and energy demand could result in significant degradation of natural vegetation. Tilman et al. (2001) projected an 18% increase in global agricultural (cropland & pastureland) area in 2050 relative to 2000. By 2050 (IPCC A1B scenario), significant degradation of natural vegetation for agricultural purposes is predicted in Eastern US, Central Africa, Southern and Equatorial Asia and Western Europe while agricultural land area could decrease in South America, East Asia, Western parts of Australia and Russia (IPCC, 2001; MNP, 2006).

The changes in vegetation type and density associated with future land use/land cover change could have a direct influence on future wildfire activity. Huang et al. (2015) predicted a 15% increase in global wildfire frequency in 2050 due to land cover change alone with major increases in Africa and North America. On the contrary, land use change could result in significant declines in fire occurrence in Africa and Western US whereas increases are predicted in Australia and South America (Huang et al., 2015). Furthermore, Hg emissions from wildfires are affected by the Hg content in the vegetation (biomass) (Biswas et al., 2007) making Hg emissions particularly sensitive to future alterations in land use and land cover. In addition to land use/land cover change, future changes in climate would also influence global fire activity. Predicted warmer temperatures in the future together with alterations in precipitation patterns driven by climate change could result in significantly different fire regimes from the 2000s (Cochrane and Barber, 2009; Flannigan et al., 2009; Yue et al., 2013). Huang et al. (2015) predicted a 19% increase in global fire frequency in 2050 caused by changes in meteorology due to climate change. Yue et al. (2013) predicted that summertime surface aerosol concentrations resulting from wildfire emissions over the Western US could increase by 46–70% for organic carbon and 20–27% for black carbon by 2050 relative to the 2000s driven by climate change. Finally, the changes in anthropogenic emissions of Hg can significantly affect Hg emissions from wildfires by affecting the atmospheric deposition of Hg. Because atmospheric deposition is a major source of Hg enrichment in terrestrial vegetation and

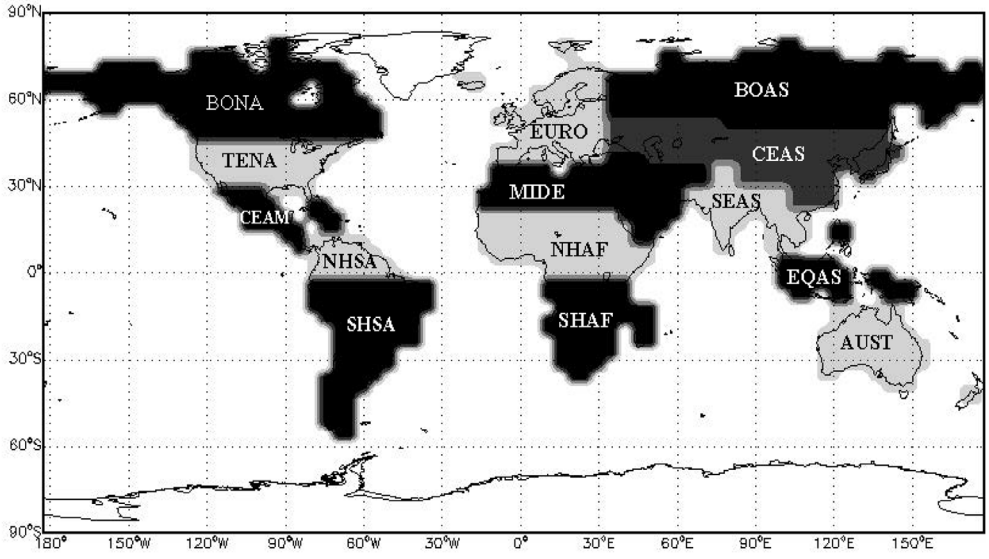

Fig. 1. Definition of global regions used in this study. BONA: Boreal North America, TENA: Temperate North America, CEAM: Central North America, NHSA: Northern Hemisphere South America, SHSA: Southern Hemisphere South America, EURO: Europe, MIDE: Middle East, NHAF: Northern Hemisphere Africa, SHAF: Southern Hemisphere Africa, BOAS: Boreal Asia, CEAS: Central Asia, SEAS: South East Asia, EQAS: Equatorial Asia, AUST: Australia.

soils, future alterations in Hg atmospheric deposition to terrestrial environments could play a key role in determining the emission factors of Hg from wildfires. In this study, we estimate the atmospheric Hg emissions from global wildfires by accounting for the regional variations in both fire activities and Hg emission factors and examining the impacts from 2000 to 2050 changes in climate, land use/land cover and anthropogenic emissions.

2. Methodology

Hg emissions from wildfires are calculated based on the classical equation for biomass burning emissions (Seiler and Crutzen, 1980) and accounting for various factors including vegetation type and density, Hg content in biomass, and fire characteristics. Considering the significant variation in fire characteristics, land cover and climate across geographical regions, the analyses for various regions is carried out separately. We use geographical region definitions that have been commonly used in the literature (Aldersley et al., 2011; Friedli et al., 2009; Giglio et al., 2010, 2013, 2006b; Li et al., 2012; Van der Werf et al., 2010; van der Werf et al., 2006).

Fig. 1 shows a map of the geographical regions. The Hg emissions model is developed at a spatial resolution of 4° × 5° (latitude x longitude). The monthly mean Hg emissions from wildfires at a grid cell (i, j), $E_{(i,j)}$, are calculated as:

$$\mathbf{E}_{(i,j)} = \sum_{k=1}^{9} \mathbf{EF}_{k(i,j)} * \mathbf{M}_{k(i,j)} * \left(\left(\frac{\mathbf{f}_{k(i,j)}}{\sum_{k=1}^{9} \mathbf{f}_{k(i,j)}} \right) * \mathbf{A}_{(i,j)} \right) * \mathbf{CF}_{(i,j)} \quad (1)$$

Where:

$\mathbf{EF}_{k(i,j)}$: Hg emission factors for land cover type k at grid cell (i, j)
$\mathbf{A}_{(i,j)}$: Burned area at (i, j)
$\mathbf{f}_{k(i,j)}$: Fractional areal coverage for land cover type k at (i, j)
$\mathbf{M}_{k(i,j)}$: Available biomass density for vegetation type k at grid cell (i, j)
$\mathbf{CF}_{(i,j)}$: Combustion fraction at (i, j)

For Hg emission factors for the 2000s, we follow Friedli et al. (2009) to assign region-specific EFs for various regions but update the tropical forests EFs with data from Melendez-Perez et al. (2014). The final EF (122 ng Hg/g biomass burned) for tropical forests is the average of values reported by Friedli et al. (2009) (198 ng Hg/g biomass burned) and Melendez-Perez et al. (2014) (47 ng Hg/g biomass burned). Boreal regions (BONA and BOAS) and Equatorial Asia (EQAS) have the highest EF values (315 ng Hg/g biomass burned) due to high soil mercury pools present there (Friedli et al., 2009) followed by temperate forests (242 ng Hg/g biomass burned), tropical forests (122 ng Hg/g biomass burned) and grasslands (41 ng Hg/g biomass burned).

Available biomass density (M) is the amount of dead/live plant material available for consumption by fires per unit area. The available biomass in a grid cell includes herbaceous vegetation, non-woody and woody tree parts and plant litter (decomposable and resistant). Available biomass estimates for forest and non-forest ecosystems from Jain et al. (2006), generated using the terrestrial component of the Integrated Science Assessment Model (ISAM) (Jain and Yang, 2005) are used here. These estimates are provided for nine geographical regions and four land cover types (tropical, temperate, boreal forests and non-forested ecosystems). Combustion fraction (CF) represents the fraction of available biomass that burns during a fire. It is a function of vegetation type, its spatial arrangement and moisture content (Ito and Penner, 2004). We follow the scheme used by Wiedinmyer et al. (2006) to estimate the CF. This scheme, based on the percentage of tree cover (TC) in a grid cell, classifies the vegetation into different types and assigns corresponding CF estimates for trees and herbaceous vegetation therein, as:

$$\mathbf{CF} = \begin{cases} 0.30 \textit{ for trees and } 0.90 \textit{ for herbs} & \textit{if } \%TC > 60\% \\ 0.30 \textit{ for trees and } \exp^{-0.013 * \%TC} \textit{ for herbs} & \textit{if } 40\% \le \%TC \le 60\% \\ 0.00 \textit{ for trees and } 0.98 \textit{ for herbs} & \%TC < 40\% \end{cases} \quad (2)$$

Land cover data used in this work consists of fractional areal vegetation coverage output (2000 and 2050) from the Lund-Potsdam Jena Dynamic Global Vegetation (LPJ DGVM) model (Gerten et al., 2004; Hickler et al., 2006; Schaphoff et al., 2006; Sitch et al., 2003; Thonicke et al., 2001; Wu et al., 2012). The LPJ model is a process based global model of vegetation dynamics. It simulates the production and loss of plant biomass, competition amongst different plant species for resources, vegetation structural properties and soil biogeochemistry (Gerten et al., 2004; Thonicke et al., 2001) based on the inputs of meteorology, soil type and atmospheric CO_2 concentration. Natural vegetation in each grid cell is described in terms of fractional coverage of 9 plant functional types (PFTs), which include *tropical broadleaved evergreen tree (TrBE)*, *tropical broadleaved raingreen tree (TrBR)*, *temperate needleleaved evergreen tree (TeNE)*, *temperate broadleaved evergreen tree (TeBE)*, *temperate broadleaved summergreen tree (TeBS)*, *boreal needleleaved evergreen tree (BNE)*, *boreal needleleaved summergreen tree (BNS)*, *C3 and C4 herbs*. Each woody PFT is either evergreen, summergreen or raingreen depending on water availability and temperature whereas herbaceous PFTs are C3 or C4 based on the type of photosynthesis activity associated with them. The fractional natural vegetation coverage output used here was obtained by driving the LPJ DGVM with meteorology fields (2000 and 2050) generated from the GISS Global Climate Model Version 3 (GISS GCM v3) (Rind et al., 2007; Wu et al., 2007, 2008a, 2008b) following the IPCC A1B scenario for future greenhouse gas concentrations. Further simulation details are provided in Wu et al. (2012). Here 10-year average vegetation data (1991–2000 vs 2041–2050) is used to examine the long-term changes in vegetation.

Data for anthropogenic land use consists of cropland areal coverage (2000 and 2050) from the IMAGE model following the IPCC A1B scenario (IMAGE Team, 2001; MNP, 2006). The data was regridded from a spatial resolution of 1° × 1°–4° × 5° in this work. For each grid cell, fractional coverage of each of the LPJ PFTs was uniformly reduced in proportion to the crop fraction to accommodate for cropland coverage. For the 2000s, the LPJ PFT and crop fractions are at the 2000s level. The 2000–2050 land use and land cover scenario includes both natural vegetation and crop coverage as predicted for 2050. The land cover change scenario has natural vegetation changing in response to climate change but the cropland coverage is kept fixed at the 2000s level whereas in the land use change scenario natural vegetation is kept fixed at the 2000s level and cropland coverage following land use trends for 2050 is used. The climate change scenario involves changes in meteorology only (using GISS GCM v3 meteorology fields for 2000 and 2050).

The burned area $\mathbf{A}_{(i,j)}$ was estimated as:

$$\mathbf{A}_{(i,j)} = \alpha_{(i,j)}\left(\mathbf{T}_{f(i,j)},\ \mathbf{H}_{f(i,j)},\ \mathbf{B}_{f(i,j)},\ \mathbf{T}_{s(i,j)},\ \mathbf{P}_{s(i,j)}\right) * \mathbf{N}_{c(i,j)} \quad (3)$$

where the proportionality factor $\alpha_{(i,j)}$ is a function of land cover type and coverage (represented by tree cover ($\mathbf{T}_{f(i,j)}$), herb cover ($\mathbf{H}_{f(i,j)}$) and barren land $\mathbf{B}_{f(i,j)}$ in grid cell (i, j)) and climate (represented by surface temperature $\mathbf{T}_{s(i,j)}$ and precipitation $\mathbf{P}_{s(i,j)}$ in grid cell (i, j)). N_c is the fire frequency which is affected by fire ignition sources such as lightning strikes and anthropogenic ignitions, meteorological conditions, vegetation density and human population density. Huang et al. (2015) accounted for all these factors and estimated the changes in fire frequency (at a spatial resolution of 4° × 5° and monthly temporal resolution) in response to changes in climate, land cover, land use and population density considering a suite of scenarios (land use/land cover change,

climate change, changes in ignition agents and anthropogenic suppression of fires). Their results for the 2050 climate change, land use and land cover change scenarios are used here.

Our burned area estimation methodology involves building a statistical model relating fire activity (independent variable) and burned area (dependent variable), which was subsequently used with the fire model generated fire frequencies to predict burned area (for 2000 and 2050). We use available global fire frequencies and burned area datasets from satellite observations and consider land cover (% tree cover (% TC), % herb cover (% HC) and % barren land (% BL)) and meteorology (T_s and P_s) as the major factors influencing the relationship between fire activity and burned area. In order to account for this dependence, regression tree models are employed. A regression tree is a decision tree based statistical model (Breiman et al., 1984; Breiman and Meisel, 1976; Loh, 2008, 2011). It recursively partitions the input data space {y, x_1, ...x_n}(y is the dependent variable and x's are the independent variables) consisting of training data for the dependent and independent variables into subsets and fits separate linear regression models to each subset. The independent variables can be used as splitting variables (used to make univariate splits at each node of the tree), predictive variables (used to predict the dependent variable) or both. The splitting of input data space into subsets allows application of regression relations to a homogeneous data space with respect to the splitting variables and thus improve the applicability of the relations to the data space. The dependence of burned area on land cover has been highlighted by Van Der Werf et al. (2003) and Giglio et al. (2006b) and regression trees for predicting global burned area from fire frequencies have been previously used [e.g (Giglio et al., 2006b, 2010).]. Separate regression trees were developed for each of the 14 geographical regions in Fig. 1. This approach allows modeling the effects of fuel type (tree/herbaceous), configuration and availability and favorable/unfavorable weather conditions on wildfire spread.

The splitting variables include %TC, %HC, %BL, T_s and P_s. Each terminal node of the tree consists of a linear regression model with fire frequencies as the independent variable and burned area as the dependent variable. Training data used for constructing the regression trees is described below. Observed fire frequencies (2001–2015) are from the Collection 5 Terra MODIS Climate Modeling Grid (CMG) fire product (data at ftp://fuoco.geog.umd.edu/modis/C5/cmg/) available at a 0.5° × 0.5° spatial and monthly temporal resolution (Giglio et al., 2006a; Justice et al., 2002). For burned area, estimates from the Global Fire Emissions Database Version 4 (GFEDv4) (data at ftp://fuoco.geog.umd.edu/gfed4/monthly/) ((2001–2015)) (Giglio et al., 2013) are used. The spatial resolution of this product is 0.5° × 0.5° (monthly temporal resolution). Both datasets were regridded to a 4° × 5° spatial resolution for use in this work. LPJ land cover data (accounting for cropland coverage as described earlier) was used for the 2000s land cover. The PFTs were combined to obtain %TC (sum of all tree PFTs), % HC (sum of all herbaceous PFTs) and the remainder after accounting for natural vegetation and cropland yielded the %BL (non-vegetated land). Surface temperature and precipitation datasets consisted of monthly means generated from 3 hourly averaged (A-3) fields from the GEOS-4 (2001–2003) (Suarez et al., 2005), GEOS-5 (2004–2012) (Rienecker, 2008) and hourly average (A-1) fields from the GEOS-FP (2013–2015) (Lucchesi, 2013; Molod et al., 2012) meteorology products (4° × 5° spatial resolution). The datasets for MODIS fire frequency, GFEDv4 burned area, LPJ land cover and GEOS meteorology at 4° × 5° were prepared for each of the 14 geographical regions as defined in Fig. 1. Thus, training data for each regional regression tree consisted of a 15-year (2001–2015) time series of MODIS Terra fire frequencies, GFEDv4 burned area estimates, LPJ land cover data for the 2000s and GEOS meteorology fields. These data were used to construct regression trees for each of the 14 geographical regions. Subsequently, these regression tree models were applied to estimate the monthly-burned area for 2000 and 2050 scenarios based on fire frequencies estimated from the fire model along with land cover data from the LPJ model and surface temperature and precipitation fields (monthly means from 3 hourly averaged (A-3) fields) from the GISS GCM v3 model. With all the input data available, the Hg emissions (with monthly and 4° × 5° resolution) from wildfires for various regions and scenarios are calculated using the fire emissions model (i.e. Eq. (1)).

To examine the perturbations to wildfire emissions of Hg from changes in anthropogenic emissions of Hg, we assume a linear relationship between the Hg emission factors from wildfires and the atmospheric deposition of mercury (Dep): $EF_{2000}/DEP_{2000} = EF_{2050}/DEP_{2050}$. The actual response of Hg enrichment in vegetation and soils to changes in atmospheric deposition could be very complicated and non-linear, but without detailed data available, the linear simplification allows us to estimate the sensitivity of wildfire emissions of Hg to changes in anthropogenic emissions. The atmospheric deposition of mercury for the 2000s and 2050 were estimated using the global mercury simulation in the GEOS-Chem model (Bey et al., 2001). The GEOS-Chem mercury simulation (Corbitt et al., 2011; Giang et al., 2015; Holmes et al., 2010; Jaeglé et al., 2009; Selin and Jacob, 2008; Selin et al., 2007, 2008; Smith-Downey et al., 2010; Strode et al., 2007; Zhang et al., 2016) includes three Hg species (elemental (Hg (0)), divalent (Hg (II)) and particulate bound Hg (Hg (P)). It includes coupled land-ocean-atmosphere cycling of Hg. Hg emissions include anthropogenic and natural sources and re-emission of previously deposited mercury from terrestrial and aquatic systems. Sinks for Hg include dry deposition, wet deposition (for Hg (II) and Hg (P)) including sea salt uptake (for Hg (II)). This work uses v9-02 of the model and years 2005–2011 were simulated with the GEOS-5 meteorology. The years 2005–2007 were used to initialize the model and the results presented are averages for 2008–2011. The model was driven by anthropogenic emissions for 2050 following the IPCC A1B scenario (Corbitt et al., 2011; Streets et al., 2009). Hg GDEP was calculated as the sum of deposition for all Hg species (Hg (0), Hg (II) and Hg (P) dry deposition + Hg (II) and Hg (P) wet deposition).

3. Results

3.1. Burned area estimates

Using the regression tree models described above, the calculated 2000s (1998–2002 average) annual burned area estimates for various regions, are shown in Table 1a. The regression tree models were able to explain most of the variability in burned area (based on GFEDv4 data) for each region (R^2 = 0.81 (BONA), 0.72 (TENA), 0.68 (CEAM), 0.75 (NHSA), 0.86 (SHSA), 0.82 (EURO), 0.81 (MIDE), 0.91 (NHAF), 0.94 (SHAF), 0.81 (BOAS), 0.85 (CEAS), 0.73 (SEAS), 0.77 (EQAS), 0.96 (AUST)). Global annual burned area for the 2000s is estimated at ~334 Mha $year^{-1}$ with maximum (51%) contribution from the African continent (MIDE + NHAF + SHAF ~170 Mha $year^{-1}$) followed by Eurasia (23%) (EURO + BOAS + CEAS + SEAS + EQAS ~ 78 Mha $year^{-1}$), South America (14%) (NHSA + SHSA ~ 47 Mha $year^{-1}$), Australia (9%) (AUST ~ 29 Mha $year^{-1}$) and North America (3%) (BONA + TENA + CEAM ~10 Mha $year^{-1}$). Table 1a contains burned area estimates from this work together with available literature estimates for comparison. There is considerable variability in the global and continental burned area estimates in the literature due to different approaches used (e.g., process based fire modeling vs. satellite observations) and different year/time period examined. However, our results reproduce the major burned area patterns common to most of the studies (e.g. maximum-burned area in Africa). Overall, estimates of both global and regional wildfire burned area in this work are in reasonable agreement with the literature and represent the spatial distribution of burned area well.

Our calculated changes in wildfire burned area driven by changes in climate, land use, land cover are shown in Table 1b. We find that the 2000–2050 climate change could increase the global fire frequencies by 19% (Huang et al., 2015), which would cause significant increases in burned area at both global (+22%) and regional (Africa (+28%),

Table 1a
Estimated regional[a] and global wildfire burned area (in Mha year^{-1}) for the 2000s.

Study	Study period	NA	SA	AFR	EURAS	AUS	GLOB
This work	**1998–2002**	**10**	**47**	**170**	**78**	**29**	**334**
GFEDv4 (Giglio et al., 2013)	1996–2015	6	21	238	28	49	342
GFEDv3 (Giglio et al., 2010)	1997–2011	5	23	253	30	52	363
GLOBSCAR 2000 (Simon et al., 2004)	2000	11.1		121		18	200
GBA 2000[b], (Tansey et al., 2004a) (Tansey et al., 2004b)	2000	7	10.5	224	52.5	56	350
L3JRC (Tansey et al., 2008)	2000–2007						392
(Randerson et al., 2012)	2000–2010	8.7	33.8	323.7	49.5	48.5	464.3
Li et al. (2012)	1997–2004			180			330
MCD45A1 (Roy et al., 2008)	2002–2010						338
FINNv1 (Wiedinmyer et al., 2011)	2005–2010	18.4	74.5	302.9	64.7	16.6	477.1

[a] Regional definitions: NA = North America (BONA + TENA + CEAM); SA = South America (NHSA + SHSA); AFR = Africa (MIDE + NHAF + SHAF); EURAS = Eurasia (Europe (EURO) + Asia (BOAS + CEAS + SEAS + EQAS)); AUS = Australia (AUST); GLOB = global total. The subcontinental regions such as BONA etc. are as defined in Fig. 1.

[b] Continental estimates calculated from percent distribution in Tansey et al. (2004b) [North America: 2%, South America: 3%, Eurasia (Europe + Asia (including Russia)): 15%, Africa: 64%, Australia + Papua New Guinea: 16%].

Table 1b
Projected 2000–2050 changes in wildfire burned area driven by changes in climate, land use, and land cover at global and regional[a] scales. Estimated burned area for the 2000s is shown in Mha year^{-1}.

Scenario	NA	SA	AFR	EURAS	AUS	GLOB
2000s	10	47	170	78	29	334
climate change	+23%	+16%	+28%	+6%	+32%	+22%
land use change	−13%	+12%	−7%	−13%	+31%	−3%
land cover change	+28%	+2%	+16%	−3%	−5%	+8%
land use and land cover change	+16%	+18%	+6%	−11%	+32%	+6%

[a] The regional definitions are the same as in Table 1a.

Australia (+32%), North America (+23%), South America (+16%) and Eurasia (+6%)) scales. An increase of 6% (+8% (land cover change), −3% (land use change)) in global burned area is predicted due to the 2000–2050 changes in land use/land cover. However, at the continental scale, more pronounced changes are observed. Burned area in North America and Africa is predicted to decline by 13% and 7% respectively due to reduction in natural vegetation coverage caused by agricultural land expansion. Lesser natural vegetation coverage could significantly reduce wildfire activity and limit wildfire spread. On the other hand, greater vegetation density and the resulting higher fire frequencies due to land cover change could increase burned area in both continents (+28% North America, +16% Africa). Agricultural land expansion is predicted to decline in South America and Australia by 2050 resulting in more natural vegetation and greater fire frequencies increasing the burned area by 12% and 31% respectively. In Eurasia, burned area could decline by 13% due to increase in agricultural land coverage. The combined effects of 2000–2050 land use/land cover change contribute to greater burned area in all continents (North America (+16%), South America (+18%), Africa (+6%), Australia (+32%)) except Eurasia (−11%).

3.2. Hg emissions from wildfires for the 2000s

Our calculated Hg emissions from wildfires for the 2000s are shown in Table 2. Results from previous literature on Hg emissions from biomass burning are included in the table for comparison. Our best estimated global total Hg wildfire emissions for the 2000s is 612 Mg year^{-1} with 43.8% emissions from the African continent (MIDE + NHAF + SHAF = 268 Mg year^{-1}) followed by Eurasia (EURO + BOAS + CEAS + SEAS + EQAS = 31%, 190 Mg year^{-1}), South America (NHSA + SHSA = 16.6%, 102 Mg year^{-1}), North America (BONA + TENA + CEAM = 7.9%, 48 Mg year^{-1}) and Australia (AUST = 0.7%, 4 Mg year^{-1}). Africa and Eurasia are the dominant source regions for Hg emissions from wildfires. High emissions from Africa can be attributed to the high fire activity, which results in more than half of the global burned area occurring in the continent. The significant contribution from Eurasia primarily reflects the high Hg pools present over the boreal parts of the continent (Friedli et al., 2009). Globally, tropical (43.3%) and boreal (33%) forest burning contribute the most to wildfire emissions of Hg followed by temperate forests (16.4%) and grasslands (7.3%).

The calculated global total wildfire emissions of Hg in this work compare very well with the climatological values reported in the literature. However, at the continental scale, there are some significant differences. Equatorial Asia is not the major source of wildfire emissions of Hg, as found by Friedli et al. (2009). In addition, the calculated emissions for Africa are much higher, although we follow the same regional emission factor assignment methodology used by them. This could be due to differences in other inputs to the fire emissions model (e.g. predicted burned area from simulated fire frequencies, available biomass density and different combustion fraction schemes used). The calculated global Hg emissions and the source distribution show much better agreement with Streets et al. (2009) with Africa being the most important source region followed by Eurasia + Oceania and South America.

Our fire emissions model uses inputs from a large number of data sources. For example, the values for Hg emission factors are average values that have been compiled from several studies in the literature; estimates of the burned area involves regression tree models, which were developed based on data from MODIS-Terra, GFEDv4, the LPJ model as well as the GEOS meteorology. Thus, it is very difficult to quantify the uncertainty in our final results associated with all the model parameters. Nevertheless, we have carried out some simple analyses to examine the sensitivities of our results to various model parameters. We first use the bootstrap methods (Efron, 1979; Efron and Tibshirani, 1993) to evaluate the uncertainties in our calculated Hg emissions from wildfires associated with the inter-annual variability in meteorology. Bootstrap methods belong to the class of nonparametric Monte Carlo methods. In this work, nonparametric bootstrapping is used which regards the data sample as the pseudo-population distribution with similar characteristics as the true population. It involves estimating the sampling distribution of a statistic (e.g. mean of the sample) by repeated sampling (with replacement) from the data sample and subsequent determination of the properties of the statistic (e.g. standard error of the mean). We apply bootstrap methods to the 5-year (1998–2002) emissions sample (global and continental) to determine the standard error of the mean as a measure of the uncertainty in the emissions. In order to provide a range for the mean, the 95% better bootstrap confidence intervals (BCa) (Efron and Tibshirani, 1993) are reported. Random samples (size n = 5) were selected from the original emissions sample and the mean was calculated. This procedure was repeated 10,000 times to create a sample of 10,000 means. The standard deviation of these 10,000 means (standard error (SE) of the mean)

Table 2
Model calculated 2000s wildfire emissions of Hg (in Mg year^{-1}) for the global total and various regions.[a,b]

Study	Study Period	NA	SA	AFR	EURAS	AUS	GLOB
This work	**1998–2002**	**48**	**102**	**268**	**190**	**4**	**612**
Brunke et al. (2001)							510–1 140[c] 380–1 330[d]
Chen et al. (2013)[e]	2000–2010				6.20		
Cinnirella and Pirrone (2006)[f]					4.3–28.4		
Delacerda (1995)[g]			17				
De Simone et al. (2015)	2006–2010						600–678
Ebinghaus et al. (2007)	1996–2000						210–750
Friedli et al. (2009)	1997–2006	50	108	141	357	19	675 (435–915)
Huang et al. (2011)[e]	2000–2007				27		
Michelazzo et al. (2010)[g]	2000–2008		7				
Nelson et al. (2012)	2006					21–63	
Roulet et al. (1999)[g]	(range for the 1980s)		6–9				
Sigler et al. (2003)							250–430
Streets et al. (2009)	(for 1996 and 2006)	28.6[h]-28.7[i]	146.9[i]-156.5[h]	252.7[h]-229[i]	176.3[h]–181.4[i]		586[i]–614[h]
Veiga et al. (1994)[g]	1988		88				
Wiedinmyer and Friedli (2007)[j]	2002–2006	44 (20–65)					
Weiss-Penzias et al. (2007)	Late 1990s						670 (340–1 000)

[a] The regional definitions are the same as in Table 1a.
[b] The specific values shown for this work represent our best estimates; refer to Table 3 and the corresponding discussion in the text for uncertainty analyses.
[c] Based on Hg/CO emission ratio.
[d] Based on Hg/CO_2 emission ratio.
[e] Emission estimates only for China.
[f] Emissions for Europe (1990–2004) and Russian federation (1996–2002) only.
[g] For Amazon only.
[h] For 1996.
[i] For 2006.
[j] Emissions for lower 48 states of North America & Alaska only.

Table 3
Sensitivity of calculated wildfire Hg emissions (in Mg year^{-1}) to various model parameters used in this study.

Region	Emission factors	Burned area	Available biomass density	Meteorology[a] (SE/Mean)
North America	44–50	41–52	44–54	46-51 (2.08%)
South America	95–120	86–116	91–109	95-111 (4.04%)
Africa	251–311	238–279	230–293	255-281 (2.51%)
Eurasia	163–197	175–203	182–202	180-199 (2.58%)
Australia	3.8–4.4	3.9–4.2	3.4–4.8	3.4–4.5 (6.75%)
Global	556–683	544–654	551–662	598-630 (1.32%)

[a] Ranges of Hg emissions represent the 95% confidence intervals.

was computed to estimate the uncertainty. The standard errors range from 1.3% to 7% (SE/mean; Table 3), reflecting the relatively small inter-annual variability in the simulated meteorology from the GISS GCM.

We then examine the sensitivities of our calculated Hg emissions from wildfires to the uncertainties in model parameters including burned area, Hg emission factors and available biomass density. Based on literature studies (e.g. Andreae and Merlet, 2001; Brunke et al., 2001; Friedli et al., 2003, 2009; Ebinghaus et al., 2007; Weiss-Penzias et al., 2007), it appears an uncertainty of 20–30% is typical for these model parameters. Therefore, we have performed two additional simulations for each model parameter by assuming a 20% uncertainty (case 1: −20 to 0% change in the parameter, case 2: 0–20% change in the parameter). For each case, a sequence of random numbers between the range [-20, 0] or [0, 20]) were generated with a uniform distribution function. These numbers represent the percentage changes to be applied to the model parameters. Therefore, for case 1, all the random numbers would be between −20 and 0 and 0 to 20 for case 2. For burned area, the random number sequence length equaled to one number representing a particular region (1: BONA, 2: TENA … 14: AUST). For emission factors and biomass density, the sequence consisted of different numbers for each vegetation type in a region. Based on these perturbation tests, we have summarized the sensitivities of our final results to various model parameters, as shown in Table 3. We find that the sensitivities of calculated Hg emissions to the three model parameters (Hg emission factors, available biomass density, and the burned area) are similar and a 20% uncertainty in each of the parameter would lead to around 20% uncertainty in our final results.

3.3. Changes in Hg emissions driven by climate, land use/land cover and anthropogenic emissions change

The perturbations to wildfire emissions of Hg due to 2000–2050 changes in climate, land use and land cover and anthropogenic emissions are shown in Fig. 2(a), Fig. 2(b) (Supplementary material) and Table 4. We find significant increases in wildfire emissions of Hg due to 2000–2050 changes in climate. Global emissions increase by 14% mainly driven by increases in Africa (+14%), South America (+18%), and Eurasia (+13%). In Africa, emissions increase mainly in the southern and northern parts, which could experience significantly warmer and drier conditions than the 2000s resulting in greater and more severe wildfires. Greater precipitation in Central Africa on the other hand causes a decline in wildfire activity and emissions. Eurasian emissions increase is primarily due to higher wildfire activity caused by warmer conditions in the boreal parts of the region (14% increase in BOAS). However, emissions in Equatorial Asia could decline due to suppression of wildfire activity caused by greater precipitation. Significant increases in wildfires is predicted over the boreal parts of North America due to warmer temperatures and over Western US due to warmer and drier conditions than the 2000s. These changes in climate result in increasing Hg emissions from North America by 8%. Australia (34% increase in emissions) and South America could mainly experience greater wildfire activity in the eastern parts due to higher temperatures and less precipitation in 2050.

In response to the projected changes in land use and land cover by 2050, we find that land use change would be a major driving force in Africa. Substantial conversion of forests to croplands causes wildfire emissions to decline by 36% in the continent, outweighing a 14%

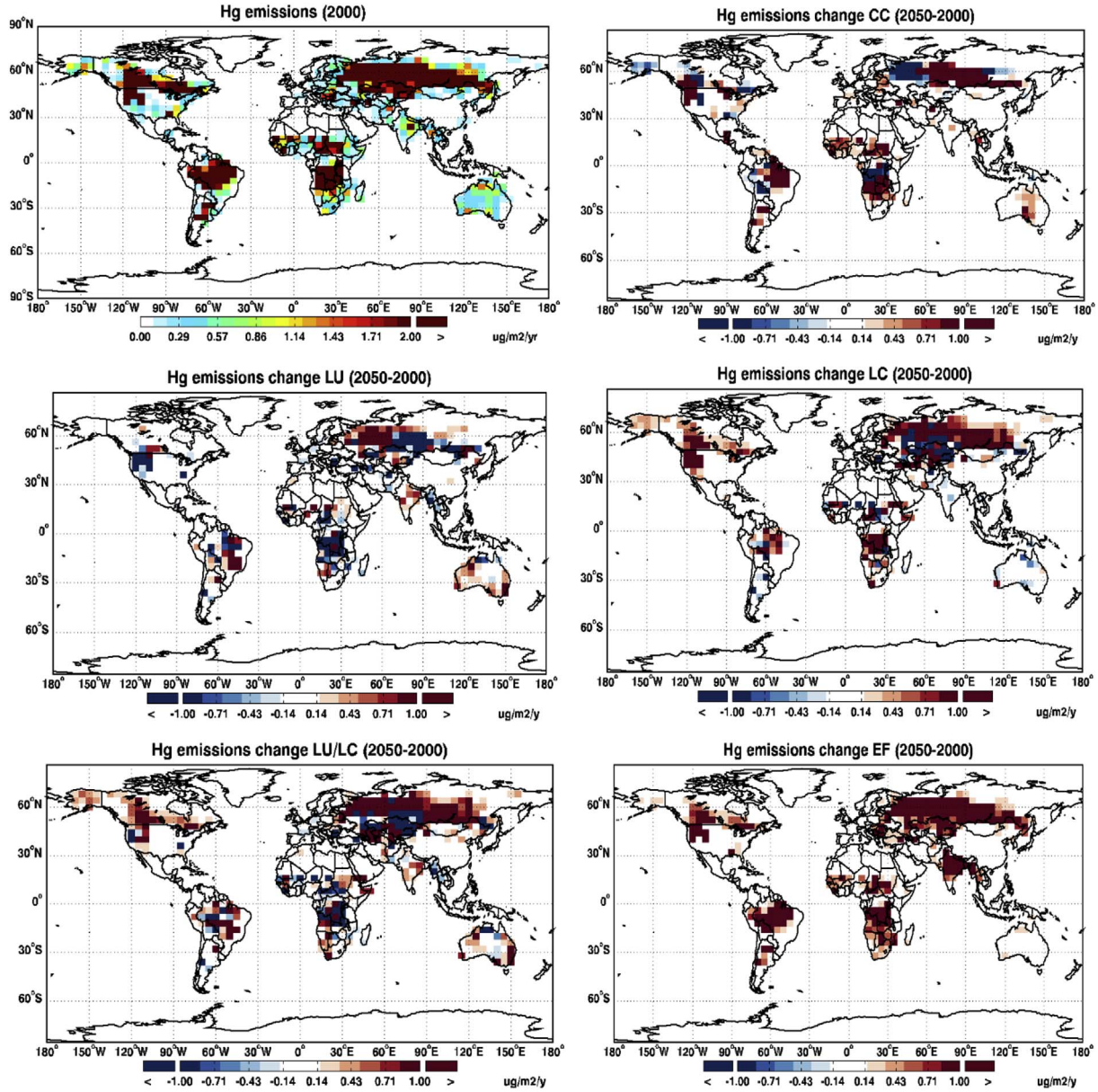

Fig. 2. (a): Wildfire emissions of Hg for 2000 (μg/m^2/year) (top left), and projected changes by 2050 (μg/m^2/year) due to climate change (CC) (top right), land use change (LU) (middle left), land cover change (LC) (middle right), land use/land cover change (bottom left) and anthropogenic emissions change (EF change) (bottom right).

Table 4
Projected 2000–2050 changes in wildfire emissions of Hg driven by changes in climate, land use, and land cover. Estimated 2000s Hg emissions are shown in Mg year^{-1}.

Scenario/Region[a]	NA	SA	AFR	EURAS	AUS	GLOB
2000s	48	102	268	190	4	612
climate change	+8%	+18%	+14%	+13%	+34%	+14%
land use change	−12%	+19%	−36%	−1%	+58%	−13%
land cover change	+32%	−5%	+14%	+13%	−11%	+12%
land use and land cover change	+19%	+21%	−24%	+17%	+182%	+0.8%
anthropogenic emissions	+19%	+20%	+24%	+41%	+18%	+28%

[a] The regional definitions are the same as in Table 1a.

increase in emissions due to greater forest coverage and resulting fire frequencies caused by land cover change. Overall, the combined effects of land use and land cover result in a 24% decline in Hg wildfire emissions from Africa. Land use change could also be the dominant factor influencing emissions in South America and Australia. Land use is projected to decline in both the continents resulting in more forest coverage and wildfires than the 2000s. Hence, emissions increase significantly in both continents (+19% (South America), +58% (Australia)). However, land cover change could cause a decline in emissions in both continents (−5% (South America), −11% (Australia)), primarily due to reduction in temperate forest (high Hg emission factors) coverage in sub-tropical South America and decrease in wildfire frequency in Australia. Overall, 2000–2050 land use/land cover change results in increasing Hg wildfire emissions by 21% in South America and 182% in Australia.

On the contrary, future changes in land cover in North America are found to have a greater influence on Hg emissions from wildfires (32% emissions increase) than the changes in anthropogenic land use (12% emissions decrease). Increase in boreal and temperate forest coverage in the high and mid-latitudes of the continent and the resulting greater fire frequencies lead to increases in Hg emissions over boreal North America (+29%) and the US (+35%). Land use change would have negligible impacts on emissions in boreal North America; however, it could result in a significant decrease in emissions from the US (−23%).

In Eurasia as well, land cover change acts as a major factor causing a 13% increase in emissions, primarily caused by boreal forest expansion and the resulting increase in wildfires. Land use change would have negligible overall effects partly reflecting the diverging trends in anthropogenic land use in this region (e.g. decreases in Eastern Asia and parts of Russia but increases in Equatorial Asia).

Following the IPCC A1B scenario, the global anthropogenic emissions are predicted to increase with Hg(II) being the dominant emissions constituent in 2050 (Corbitt et al., 2011; Streets et al., 2009). As a consequence, we find that the Hg enrichment of terrestrial ecosystems driven by changes in atmospheric Hg deposition by 2050 would lead to increases in global wildfire emissions of Hg by 28%. The most significant increases are calculated over Eurasia (+41%) and Africa (+24%) which together account for about 75% of global Hg wildfire emissions for the 2000s. Wildfire emissions of Hg from South East, Central and East Asian countries increase significantly in response to greater Hg anthropogenic emissions in these countries and the resulting deposition to terrestrial environments. South America (+20%), North America (+19%) and Australia (+18%) experience significant increases in emissions as well. Greater Hg deposition to the boreal regions results in an increase of 19% in wildfire emissions from boreal North America and 35% from boreal Asia. Emissions from tropical peatlands in Equatorial Asia also increase due to greater Hg deposition in 2050. It should be noted that new developments in technology (such as the mercury control technology being used by coal-fired power plants) and policy (such as the Minamata Convention) can significantly affect the future trends of anthropogenic emissions of Hg, but these factors are not accounted for in this study.

4. Conclusions

We investigate the Hg emissions from wildfires in this study. We first develop the global and regional emission inventories for the 2000s and then examine the perturbations from the projected 2000–2050 changes in climate, land use, land cover and anthropogenic Hg emissions. Africa (43.8%), Eurasia (31%) and South America (16.6%) are found to be the major sources of Hg wildfire emissions in the 2000s. Following the IPCC A1B scenario, 2000–2050 climate change would lead to more frequent and severe wildfires in most regions around the world resulting in significant increases in wildfire emissions of Hg at both the global and continental scales. Climate change driven alterations in natural vegetation could also increase global emissions particularly in the boreal regions, the US and Africa. However, these impacts of a future favorable climate for fires and land cover change on global emissions are suppressed by continued anthropogenic destruction of natural vegetation in order to support agricultural development. As a result, emissions in Africa, which is a major source of wildfire emissions, decline in 2050 due to reduced forest cover. In addition, destruction of forests in Equatorial Asia and the Western US reduces Hg wildfire emissions from these regions. On the other hand, a projected rise in anthropogenic emissions in 2050 and the resulting greater Hg contamination of terrestrial environments contributes to increasing emissions globally and regionally. Wildfire emissions of Hg in the boreal regions are predicted to increase in response to the 2000–2050 changes in climate, land cover and anthropogenic Hg emissions which could have significant implications for Hg deposition to the Arctic.

Conflicts of interest

The authors declare that they have no conflict of interest.

Acknowledgements

This study is supported by NSF (grant #1313755) and U.S. EPA (grant # 83518901). J.O. Kaplan was further supported by the European Research Council (COEVOLVE 313797). S. Wu acknowledges the sabbatical fellowship from Peking University. Superior, a high performance computing cluster at Michigan Technological University, was used in obtaining results presented in this publication.

Appendix A. Supplementary data

Supplementary data related to this article can be found at http://dx.doi.org/10.1016/j.atmosenv.2017.10.061.

References

Aldersley, A., Murray, S.J., Cornell, S.E., 2011. Global and regional analysis of climate and human drivers of wildfire. Sci. Total Environ. 409, 3472–3481.
Andreae, M.O., Merlet, P., 2001. Emission of trace gases and aerosols from biomass burning. Glob. Biogeochem. Cycles 15, 955–966.
Bachelet, D., Neilson, R.P., Hickler, T., Drapek, R.J., Lenihan, J.M., Sykes, M.T., Smith, B., Sitch, S., Thonicke, K., 2003. Simulating past and future dynamics of natural ecosystems in the United States. Glob. Biogeochem. Cycles 17.
Bachelet, D., Neilson, R.P., Lenihan, J.M., Drapek, R.J., 2001. Climate change effects on vegetation distribution and carbon budget in the United States. Ecosystems 4, 164–185.
Bey, I., Jacob, D.J., Yantosca, R.M., Logan, J.A., Field, B.D., Fiore, A.M., Li, Q., Liu, H.Y., Mickley, L.J., Schultz, M.G., 2001. Global modeling of tropospheric chemistry with assimilated meteorology: model description and evaluation. J. Geophys. Res. Atmos. 106, 23073–23095.
Biswas, A., Blum, J.D., Klaue, B., Keeler, G.J., 2007. Release of mercury from Rocky Mountain forest fires. Glob. Biogeochem. Cycles 21.
Breiman, L., Friedman, J., Olshen, R., Stone, C., 1984. Classification and Regression Trees. CRC Press, Boca Raton, Florida.
Breiman, L., Meisel, W., 1976. General estimates of the intrinsic variability of data in nonlinear regression models. J. Am. Stat. Assoc. 71, 301–307.
Brunke, E.G., Labuschagne, C., Slemr, F., 2001. Gaseous mercury emissions from a fire in the cape peninsula, South Africa, during january 2000. Geophys. Res. Lett. 28, 1483–1486.
Chen, C., Wang, H., Zhang, W., Hu, D., Chen, L., Wang, X., 2013. High-resolution inventory of mercury emissions from biomass burning in China for 2000–2010 and a projection for 2020. J. Geophys. Res. Atmos. 118.
Chen, Y., Wang, R., Shen, H., Li, W., Chen, H., Huang, Y., Zhang, Y., Chen, Y., Su, S., Lin, N., 2014. Global mercury emissions from combustion in light of international fuel trading. Environ. Sci. Technol. 48, 1727–1735.
Cinnirella, S., Pirrone, N., 2006. Spatial and temporal distributions of mercury emissions from forest fires in Mediterranean region and Russian Federation. Atmos. Environ. 40, 7346–7361.
Cochrane, M.A., Barber, C.P., 2009. Climate change, human land use and future fires in the Amazon. Glob. Change Biol. 15, 601–612.
Corbitt, E.S., Jacob, D.J., Holmes, C.D., Streets, D.G., Sunderland, E.M., 2011. Global source–receptor relationships for mercury deposition under present-day and 2050 emissions scenarios. Environ. Sci. Technol. 45, 10477–10484.
Cox, P.M., Betts, R.A., Jones, C.D., Spall, S.A., Totterdell, I.J., 2000. Acceleration of global warming due to carbon-cycle feedbacks in a coupled climate model. Nature 408, 184–187.
De Simone, F., Cinnirella, S., Gencarelli, C.N., Yang, X., Hedgecock, I.M., Pirrone, N., 2015. Model study of global mercury deposition from biomass burning. Environ. Sci. Technol. 49, 6712–6721.
Delacerda, L.D., 1995. Amazon mercury emissions. Nature 374, 20–21.
Ebinghaus, R., Slemr, F., Brenninkmeijer, C., Van Velthoven, P., Zahn, A., Hermann, M., O'Sullivan, D., Oram, D., 2007. Emissions of gaseous mercury from biomass burning in South America in 2005 observed during CARIBIC flights. Geophys. Res. Lett. 34.
Efron, B., 1979. Bootstrap methods: another look at the jackknife annals of statistics. 7, 1–26.
Efron, B., Tibshirani, R.J., 1993. An Introduction to the Bootstrap: Monographs on Statistics and Applied Probability, vol. 57 Chapman and Hall/CRC, New York and London.
Falloon, P., Dankers, R., Betts, R., Jones, C., Booth, B., Lambert, F., 2012. Role of vegetation change in future climate under the A1B scenario and a climate stabilisation scenario, using the HadCM3C Earth system model. Biogeosciences 9, 4739.
Ferrara, R., Mazzolai, B., Lanzillotta, E., Nucaro, E., Pirrone, N., 2000. Volcanoes as emission sources of atmospheric mercury in the Mediterranean basin. Sci. Total Environ. 259, 115–121.
Flannigan, M.D., Krawchuk, M.A., de Groot, W.J., Wotton, B.M., Gowman, L.M., 2009. Implications of changing climate for global wildland fire. Int. J. Wildland Fire 18, 483–507.
Friedli, H., Arellano, A., Cinnirella, S., Pirrone, N., 2009. Initial estimates of mercury emissions to the atmosphere from global biomass burning. Environ. Sci. Technol. 43, 3507–3513.
Friedli, H., Radke, L., Lu, J., Banic, C., Leaitch, W., MacPherson, J., 2003. Mercury emissions from burning of biomass from temperate North American forests: laboratory and airborne measurements. Atmos. Environ. 37, 253–267.
Gerten, D., Schaphoff, S., Haberlandt, U., Lucht, W., Sitch, S., 2004. Terrestrial vegetation and water balance—hydrological evaluation of a dynamic global vegetation model. J. Hydrol. 286, 249–270.
Giang, A., Stokes, L.C., Streets, D.G., Corbitt, E.S., Selin, N.E., 2015. Impacts of the

minamata convention on mercury emissions and global deposition from coal-fired power generation in Asia. Environ. Sci. Technol. 49, 5326–5335.
Giglio, L., Csiszar, I., Justice, C.O., 2006a. Global distribution and seasonality of active fires as observed with the Terra and aqua moderate resolution imaging spectroradiometer (MODIS) sensors. J. Geophys. Res. Biogeosci. 111.
Giglio, L., Randerson, J., Van der Werf, G., Kasibhatla, P., Collatz, G., Morton, D., DeFries, R., 2010. Assessing variability and long-term trends in burned area by merging multiple satellite fire products. Biogeosciences 7.
Giglio, L., Randerson, J.T., Werf, G.R., 2013. Analysis of daily, monthly, and annual burned area using the fourth-generation global fire emissions database (GFED4). J. Geophys. Res. Biogeosci. 118, 317–328.
Giglio, L., Van der Werf, G., Randerson, J., Collatz, G., Kasibhatla, P., 2006b. Global estimation of burned area using MODIS active fire observations. Atmos. Chem. Phys. 6, 957–974.
Graydon, J.A., St Louis, V.L., Lindberg, S.E., Sandilands, K.A., Rudd, J.W., Kelly, C.A., Harris, R., Tate, M.T., Krabbenhoft, D.P., Emmerton, C.A., 2012. The role of terrestrial vegetation in atmospheric Hg deposition: pools and fluxes of spike and ambient Hg from the METAALICUS experiment. Glob. Biogeochem. Cycles 26.
Hickler, T., Prentice, I.C., Smith, B., Sykes, M.T., Zaehle, S., 2006. Implementing plant hydraulic architecture within the LPJ dynamic global vegetation model. Glob. Ecol. Biogeogr. 15, 567–577.
Holmes, C.D., Jacob, D.J., Corbitt, E.S., Mao, J., Yang, X., Talbot, R., Slemr, F., 2010. Global atmospheric model for mercury including oxidation by bromine atoms. Atmos. Chem. Phys. 10, 12037–12057.
Huang, X., Li, M., Friedli, H.R., Song, Y., Chang, D., Zhu, L., 2011. Mercury emissions from biomass burning in China. Environ. Sci. Technol. 45, 9442–9448.
Huang, Y., Wu, S., Kaplan, J.O., 2015. Sensitivity of global wildfire occurrences to various factors in the context of global change. Atmos. Environ. 121, 86–92.
IMAGE Team, H., 2001. The IMAGE 2.2 Implementation of the SRES Scenarios: a Comprehensive Analysis of Emissions, Climate Change and Impacts in the 21st Century. RIVM CD-ROM Publication 481508018.
IPCC, 2001. Climate change 2001: the scientific basis, contribution of working group I to the third assessment report of the intergovernmental panel on climate change. In: Houghton, J.T., Ding, Y., Griggs, D.J., Noguer, M., Linden, van der, P.J. (Eds.), Cambridge United Kingdom and New York. Cambridge University Press, NY, USA.
Ito, A., Penner, J.E., 2004. Global estimates of biomass burning emissions based on satellite imagery for the year 2000. J. Geophys. Res. Atmos. 109.
Jaeglé, L., Strode, S.A., Selin, N.E., Jacob, D.J., 2009. The Geos-chem Model, Mercury Fate and Transport in the Global Atmosphere. Springer, pp. 533–545.
Jain, A.K., Tao, Z., Yang, X., Gillespie, C., 2006. Estimates of global biomass burning emissions for reactive greenhouse gases (CO, NMHCs, and NOx) and CO2. J. Geophys. Res. Atmos. 111.
Jain, A.K., Yang, X., 2005. Modeling the effects of two different land cover change data sets on the carbon stocks of plants and soils in concert with CO2 and climate change. Glob. Biogeochem. Cycles 19.
Justice, C., Giglio, L., Korontzi, S., Owens, J., Morisette, J., Roy, D., Descloitres, J., Alleaume, S., Petitcolin, F., Kaufman, Y., 2002. The MODIS fire products. Remote Sens. Environ. 83, 244–262.
Li, F., Zeng, X., Levis, S., 2012. A process-based fire parameterization of intermediate complexity in a Dynamic Global Vegetation Model. Biogeosciences 9, 2761–2780.
Loh, W.Y., 2008. Classification and Regression Tree Methods. Encyclopedia of Statistics in Quality and Reliability.
Loh, W.Y., 2011. Classification and regression trees. Wiley Interdiscip. Rev. Data Min. Knowl. Discov. 1, 14–23.
Lucchesi, R., 2013. File Specification for GEOS-5 FP (Forward Processing).
Melendez-Perez, J.J., Fostier, A.H., Carvalho, J.A., Windmöller, C.C., Santos, J.C., Carpi, A., 2014. Soil and biomass mercury emissions during a prescribed fire in the Amazonian rain forest. Atmos. Environ. 96, 415–422.
Michelazzo, P.A.M., Fostier, A.H., Magarelli, G., Santos, J.C., Carvalho, J.A., 2010. Mercury emissions from forest burning in southern Amazon. Geophys. Res. Lett. 37.
MNP, 2006. Integrated modelling of global environmental change, an overview of IMAGE 2.4. In: Bouwman, A.F., Kram, T., Klein Goldewijk, K. (Eds.), Netherlands Environmental Assessment Agency (MNP), Bilthoven, The Netherlands.
Molod, A., Takacs, L., Suarez, M., Bacmeister, J., Song, I.-S., Eichmann, A., 2012. The GEOS-5 Atmospheric General Circulation Model: Mean Climate and Development from MERRA to Fortuna.
Nelson, P.F., Morrison, A.L., Malfroy, H.J., Cope, M., Lee, S., Hibberd, M.L., Meyer, C.M., McGregor, J., 2012. Atmospheric mercury emissions in Australia from anthropogenic, natural and recycled sources. Atmos. Environ. 62, 291–302.
Nimick, D.A., Caldwell, R.R., Skaar, D.R., Selch, T.M., 2013. Fate of geothermal mercury from yellowstone national park in the madison and Missouri rivers. USA. Sci. Total Environ. 443, 40–54.
Notaro, M., Vavrus, S., Liu, Z., 2007. Global vegetation and climate change due to future increases in CO2 as projected by a fully coupled model with dynamic vegetation. J. Clim. 20, 70–90.
Nriagu, J., Becker, C., 2003. Volcanic emissions of mercury to the atmosphere: global and regional inventories. Sci. Total Environ. 304, 3–12.
O'ishi, R., Abe-Ouchi, A., 2009. Influence of dynamic vegetation on climate change arising from increasing CO2. Clim. Dyn. 33, 645–663.
Obrist, D., 2007. Atmospheric mercury pollution due to losses of terrestrial carbon pools? Biogeochemistry 85, 119–123.
Pacyna, E.G., Pacyna, J., Sundseth, K., Munthe, J., Kindbom, K., Wilson, S., Steenhuisen, F., Maxson, P., 2010. Global emission of mercury to the atmosphere from anthropogenic sources in 2005 and projections to 2020. Atmos. Environ. 44, 2487–2499.
Pirrone, N., Cinnirella, S., Feng, X., Finkelman, R., Friedli, H., Leaner, J., Mason, R., Mukherjee, A., Stracher, G., Streets, D., 2010. Global mercury emissions to the atmosphere from anthropogenic and natural sources. Atmos. Chem. Phys. 10, 5951–5964.
Pyle, D.M., Mather, T.A., 2003. The importance of volcanic emissions for the global atmospheric mercury cycle. Atmos. Environ. 37, 5115–5124.
Randerson, J., Chen, Y., Werf, G., Rogers, B., Morton, D., 2012. Global burned area and biomass burning emissions from small fires. J. Geophys. Res. Biogeosci. 117.
Rienecker, M., 2008. File Specification for GEOS-5 DAS Gridded Output. NASA Goddard Space Flight Center.
Rind, D., Lerner, J., Jonas, J., McLinden, C., 2007. Effects of resolution and model physics on tracer transports in the NASA Goddard Institute for Space Studies general circulation models. J. Geophys. Res. Atmos. 112.
Roulet, M., Lucotte, M., Farella, N., Serique, G., Coelho, H., Sousa Passos, C., De Jesus da Silva, E., Scavone de Andrade, P., Mergler, D., Guimarães, J.-R., 1999. Effects of recent human colonization on the presence of mercury in Amazonian ecosystems. Water. Air, & Soil Pollut. 112, 297–313.
Roy, D.P., Boschetti, L., Justice, C.O., Ju, J., 2008. The collection 5 MODIS burned area product—global evaluation by comparison with the MODIS active fire product. Remote Sens. Environ. 112, 3690–3707.
Schaphoff, S., Lucht, W., Gerten, D., Sitch, S., Cramer, W., Prentice, I.C., 2006. Terrestrial biosphere carbon storage under alternative climate projections. Clim. Change 74, 97–122.
Seiler, W., Crutzen, P.J., 1980. Estimates of gross and net fluxes of carbon between the biosphere and the atmosphere from biomass burning. Clim. Change 2, 207–247.
Selin, N.E., Jacob, D.J., 2008. Seasonal and spatial patterns of mercury wet deposition in the United States: constraints on the contribution from North American anthropogenic sources. Atmos. Environ. 42, 5193–5204.
Selin, N.E., Jacob, D.J., Park, R.J., Yantosca, R.M., Strode, S., Jaeglé, L., Jaffe, D., 2007. Chemical cycling and deposition of atmospheric mercury: global constraints from observations. J. Geophys. Res. Atmos. 112.
Selin, N.E., Jacob, D.J., Yantosca, R.M., Strode, S., Jaeglé, L., Sunderland, E.M., 2008. Global 3-D land-ocean-atmosphere model for mercury: present-day versus pre-industrial cycles and anthropogenic enrichment factors for deposition. Glob. Biogeochem. Cycles 22.
Sigler, J., Lee, X., Munger, W., 2003. Emission and long-range transport of gaseous mercury from a large-scale Canadian boreal forest fire. Environ. Sci. Technol. 37, 4343–4347.
Simon, M., Plummer, S., Fierens, F., Hoelzemann, J.J., Arino, O., 2004. Burnt area detection at global scale using ATSR-2: the GLOBSCAR products and their qualification. J. Geophys. Res. Atmos. 109.
Sitch, S., Smith, B., Prentice, I.C., Arneth, A., Bondeau, A., Cramer, W., Kaplan, J., Levis, S., Lucht, W., Sykes, M.T., 2003. Evaluation of ecosystem dynamics, plant geography and terrestrial carbon cycling in the LPJ dynamic global vegetation model. Glob. Change Biol. 9, 161–185.
Smith-Downey, N.V., Sunderland, E.M., Jacob, D.J., 2010. Anthropogenic impacts on global storage and emissions of mercury from terrestrial soils: insights from a new global model. J. Geophys. Res. Biogeosci. 115.
Streets, D.G., Devane, M.K., Lu, Z., Bond, T.C., Sunderland, E.M., Jacob, D.J., 2011. All-time releases of mercury to the atmosphere from human activities. Environ. Sci. Technol. 45, 10485–10491.
Streets, D.G., Zhang, Q., Wu, Y., 2009. Projections of global mercury emissions in 2050. Environ. Sci. Technol. 43, 2983–2988.
Strode, S.A., Jaeglé, L., Selin, N.E., Jacob, D.J., Park, R.J., Yantosca, R.M., Mason, R.P., Slemr, F., 2007. Air-sea exchange in the global mercury cycle. Glob. Biogeochem. Cycles 21.
Suarez, M.J., daSilva, A., Dee, D., Bloom, S., Bosilovich, M., Pawson, S., Schubert, S., Wu, M.-L., Sienkiewicz, M., Stajner, I., 2005. Documentation and Validation of the Goddard Earth Observing System (GEOS) Data Assimilation System, Version 4.
Tansey, K., GrÉgoire, J.-M., Binaghi, E., Boschetti, L., Brivio, P.A., Ershov, D., Flasse, S., Fraser, R., Graetz, D., Maggi, M., 2004a. A global inventory of burned areas at 1 km resolution for the year 2000 derived from SPOT VEGETATION data. Clim. Change 67, 345–377.
Tansey, K., Grégoire, J.M., Defourny, P., Leigh, R., Pekel, J.F., van Bogaert, E., Bartholomé, E., 2008. A new, global, multi-annual (2000–2007) burnt area product at 1 km resolution. Geophys. Res. Lett. 35.
Tansey, K., Grégoire, J.M., Stroppiana, D., Sousa, A., Silva, J., Pereira, J., Boschetti, L., Maggi, M., Brivio, P.A., Fraser, R., 2004b. Vegetation burning in the year 2000: global burned area estimates from SPOT VEGETATION data. J. Geophys. Res. Atmos. 109.
Thonicke, K., Venevsky, S., Sitch, S., Cramer, W., 2001. The role of fire disturbance for global vegetation dynamics: coupling fire into a Dynamic Global Vegetation Model. Glob. Ecol. Biogeogr. 10, 661–677.
Tilman, D., Fargione, J., Wolff, B., D'Antonio, C., Dobson, A., Howarth, R., Schindler, D., Schlesinger, W.H., Simberloff, D., Swackhamer, D., 2001. Forecasting agriculturally driven global environmental change. Science 292, 281–284.
Turetsky, M.R., Harden, J.W., Friedli, H.R., Flannigan, M., Payne, N., Crock, J., Radke, L., 2006. Wildfires threaten mercury stocks in northern soils. Geophys. Res. Lett. 33.
Van Der Werf, G.R., Randerson, J.T., Collatz, G.J., Giglio, L., 2003. Carbon emissions from fires in tropical and subtropical ecosystems. Glob. Change Biol. 9, 547–562.
Van der Werf, G.R., Randerson, J.T., Giglio, L., Collatz, G., Mu, M., Kasibhatla, P.S., Morton, D.C., DeFries, R., Jin, Y.v., van Leeuwen, T.T., 2010. Global fire emissions and the contribution of deforestation, savanna, forest, agricultural, and peat fires (1997–2009). Atmos. Chem. Phys. 10, 11707–11735.
van der Werf, G.R., Randerson, J.T., Giglio, L., Collatz, G.J., Kasibhatla, P.S., Arellano Jr., A.F., 2006. Interannual variability in global biomass burning emissions from 1997 to 2004. Atmos. Chem. Phys. 6, 3423–3441.
Varekamp, J.C., Buseck, P.R., 1986. Global mercury flux from volcanic and geothermal

sources. Appl. Geochem. 1, 65–73.
Veiga, M.M., Maxson, P.A., Hylander, L.D., 2006. Origin and consumption of mercury in small-scale gold mining. J. Clean. Prod. 14, 436–447.
Veiga, M.M., Meech, J.A., Oñate, N., 1994. Mercury pollution from deforestation. Nature 368, 816–817.
Weiss-Penzias, P., Jaffe, D., Swartzendruber, P., Hafner, W., Chand, D., Prestbo, E., 2007. Quantifying Asian and biomass burning sources of mercury using the Hg/CO ratio in pollution plumes observed at the Mount Bachelor Observatory. Atmos. Environ. 41, 4366–4379.
Wiedinmyer, C., Akagi, S., Yokelson, R.J., Emmons, L., Al-Saadi, J., Orlando, J., Soja, A., 2011. The Fire INventory from NCAR (FINN): a high resolution global model to estimate the emissions from open burning. Geosci. Model Dev. 4, 625.
Wiedinmyer, C., Friedli, H., 2007. Mercury emission estimates from fires: an initial inventory for the United States. Environ. Sci. Technol. 41, 8092–8098.
Wiedinmyer, C., Quayle, B., Geron, C., Belote, A., McKenzie, D., Zhang, X., O'Neill, S., Wynne, K.K., 2006. Estimating emissions from fires in North America for air quality modeling. Atmos. Environ. 40, 3419–3432.
Wu, S., Mickley, L.J., Jacob, D.J., Logan, J.A., Yantosca, R.M., Rind, D., 2007. Why are there large differences between models in global budgets of tropospheric ozone? J. Geophys. Res. Atmos. 112.
Wu, S., Mickley, L.J., Jacob, D.J., Rind, D., Streets, D.G., 2008a. Effects of 2000–2050 changes in climate and emissions on global tropospheric ozone and the policy-relevant background surface ozone in the United States. J. Geophys. Res. Atmos. 113.
Wu, S., Mickley, L.J., Kaplan, J., Jacob, D.J., 2012. Impacts of changes in land use and land cover on atmospheric chemistry and air quality over the 21st century. Atmos. Chem. Phys. 12, 1597–1609.
Wu, S., Mickley, L.J., Leibensperger, E.M., Jacob, D.J., Rind, D., Streets, D.G., 2008b. Effects of 2000–2050 global change on ozone air quality in the United States. J. Geophys. Res. Atmos. 113.
Yue, X., Mickley, L.J., Logan, J.A., Kaplan, J.O., 2013. Ensemble projections of wildfire activity and carbonaceous aerosol concentrations over the western United States in the mid-21st century. Atmos. Environ. 77, 767–780.
Zhang, H., Holmes, C., Wu, S., 2016. Impacts of changes in climate, land use and land cover on atmospheric mercury. Atmos. Environ. 141, 230–244.